Three-dimensional and depth-averaged Large Eddy Simulation of Shallow Water Flows

C. Hinterberger[1], J. Fröhlich[2] & W. Rodi[1]
[1]*Inst. für Hydromechanik, Universität Karlsruhe, Germany*
[2]*Inst. für Chemische Technik, Universität Karlsruhe, Germany*

The paper presents a model for large eddy simulations (LES) of shallow flows employing depth-averaged equations. Different terms require closure such as two and three-dimensional subgrid terms, the latter comprising dispersion and isotropic contributions. These issues are discussed and corresponding models are proposed. In particular, a new stochastic backscatter model is introduced to account for the transfer of energy from the unresolved three-dimensional turbulence to the resolved two-dimensional motions. The final method as a whole is calibrated by means of a highly resolved three-dimensional LES of flow in a straight open channel performed as part of this work. Subsequently, the model is applied in computations of a plane mixing layer. The results are compared to a three-dimensional simulation and to experimental data. They show that the difficult task of capturing the Kelvin–Helmholtz–type instability in a mixed two and three-dimensional flow is realistically represented in a purely two dimensional LES by the proposed method.

Geophysical shallow flows of practical interest are characterised by a large range of scales. Often, not all these scales need to be resolved to obtain a simulation for a certain purpose (Ferziger et al. 2002). For shallow flows, depth-averaged (DA) equations have been used for some time in which turbulence is represented by a statistical turbulence model, e.g. (Guirk and Rodi 1978). However, when large-scale horizontal structures dominate the flow such models become less suited so that the LES approach appears to be beneficial. Closures for DA-LES have been proposed in the literature (Madsen et al. 1988; Nadaoka and Yagi 1998; van Vossen 2000), but these employ an eddy viscosity without any mechanism for the inverse energy transfer from the unresolved three-dimensional (3D) turbulent motion to the resolved two-dimensional (2D) motion.

In this paper we present a highly-resolved 3D-LES of flow in a straight open channel providing information about the small scale turbulence and the stresses which have to be modelled in a DA-LES. Even though there is no horizontal shear of the mean flow in this configuration, there exist energy-containing 2D structures caused by the small scale turbulence. This background 2D turbulence plays an important role in the development of larger 2D flow structures, for instance in a shallow mixing layer, where the downstream development is very sensitive to the upstream turbulence level and the spectral energy distribution (van Prooijen and Uijttewaal 2002). To model the inverse energy transfer from the unresolved 3D turbulence to the resolved 2D motion we introduce a back scatter model (BSM), which is tested on a shallow mixing layer. Due to its high sensitivity to perturbations, this flow is a good test case for DA-LES models.

1 MATHEMATICAL MODEL

1.1 THREE-DIMENSIONAL LES

For LES the Navier-Stokes equations are filtered with a spatial filter $\overline{\varphi(\mathbf{x})} = \int_D \varphi(\mathbf{x}')\, G(\mathbf{x}'-\mathbf{x}) d\mathbf{x}'$ to remove the small scales which cannot be resolved by the numerical grid employed. For a three-dimensional flow, the filtered equations read

$$\frac{\partial \overline{u_i}}{\partial x_i} = 0 \qquad (i = 1,2,3) \tag{1}$$

$$\frac{\partial \overline{u_i}}{\partial t} + \frac{\partial}{\partial x_j}\left(\overline{u_i}\,\overline{u_j}\right) = -\frac{1}{\rho}\frac{\partial \overline{p}}{\partial x_i} + \frac{\partial}{\partial x_j}\left(\nu 2\overline{S_{ij}} - \tau_{ij}\right) \tag{2}$$

where u_i is the velocity vector, $S_{ij} = 1/2\left(\partial_{x_j} u_i + \partial_{x_i} u_j\right)$ the strain-rate tensor, ρ the density, p the pressure and ν the viscosity. Filtering out the small scales gives rise to the subgrid-scale stresses $\tau_{ij}(\mathbf{u}) = \overline{u_i u_j} - \overline{u_i}\;\overline{u_j}$. Here, we use the

Smagorinsky model $\tau_{ij} - \frac{1}{3}\delta_{ij}\tau_{kk} = -\nu_t 2\overline{S_{ij}}$ with $\nu_t = (C_s\Delta)^2\sqrt{2\overline{S_{ij}}\,\overline{S_{ij}}}$ and a lengthscale $\Delta = \sqrt[3]{V}$ based on the volume of the computational cell V. Close to walls the lengthscale is reduced with a Van Driest damping function. For the Smagorinsky constant we use $C_s = 0.065$ which is appropriate for channel flow.

1.2 DEPTH-AVERAGE LES

For DA-LES Equations 1 and 2 are depth-integrated and the pressure is substituted by a hydrostatic pressure assumption yielding

$$\frac{\partial\overline{\xi}}{\partial t} + \frac{\partial}{\partial x_i}\left(h\widetilde{\overline{u_i}}\right) = 0 \qquad (i=1,2) \tag{3}$$

$$\begin{aligned}\frac{\partial(h\widetilde{\overline{u_i}})}{\partial t} &+ \frac{\partial}{\partial x_j}\left(h\,\widetilde{\overline{u_i}}\,\widetilde{\overline{u_j}}\right) = -gh\frac{\partial\overline{\xi}}{\partial x_i} \\ &+ \frac{\partial}{\partial x_j}\left(h\left(\nu 2\widetilde{\overline{S_{ij}}} - T_{ij}\right)\right) - \frac{\overline{\tau_{w_i}}}{\rho}\end{aligned} \tag{4}$$

where h, ξ, τ_w represent the water depth, the elevation of the water surface and the shear stress at the bottom, respectively. $\widetilde{(\ldots)}$ is the depth-averaging operator: $\widetilde{\varphi} = \frac{1}{h}\int_h \varphi\, dz$. Introducing a separable LES Filter leads to $\widetilde{\overline{\varphi}} = \overline{\widetilde{\varphi}}$ for a plane water surface and bottom geometry. The depth integration introduces dispersive stresses

$$D_{ij}(\mathbf{u}) = \frac{1}{h}\int_h (u_i - \widetilde{u_i})(u_j - \widetilde{u_j})\,dz = \widetilde{u_i u_j} - \widetilde{u_i}\,\widetilde{u_j} \tag{5}$$

The quantity $T_{ij}(\mathbf{u}) = \widetilde{\overline{u_i u_j}} - \widetilde{\overline{u_i}}\,\widetilde{\overline{u_j}}$ in Equation 2 is the total stress which results from combining the depth integration and the filtering. T_{ij} and the bottom shear stress τ_w need to be modelled.
For the bottom friction a quadratic friction law

$$\overline{\tau_{w_i}} = c_f\widetilde{\overline{u_i}}\left|\widetilde{\overline{\mathbf{u}}}\right| = c_f\widetilde{\overline{u_i}}\sqrt{\widetilde{\overline{u_k}}\,\widetilde{\overline{u_k}}} \tag{6}$$

can be applied. The friction coefficient c_f can be determined for a hydraulically smooth bed according to (Uijttewaal and Booij. 2000)

$$1/\sqrt{c_f} = 1/0.4\left[\ln\left(Re\sqrt{c_f}\right) + 1\right] \tag{7}$$

This implicit relation for c_f has to be solved iteratively. As this is numerically expensive we have developed the explicit relation

$$c_f = 0.0385\cdot Re^{-0.3} + 6\cdot 10^{-4} \tag{8}$$

which is equivalent to Equation 7 within a few percent in the range $2\,000 \le Re \le 10^7$. This relation is used in each time step with the local depth-based Reynolds number $Re = |\widetilde{\mathbf{u}}|\,h/\nu$ and the value $c_f = 0.00454$ for Re below $2\,000$.

Depth averaging yields $T_{ij}(\mathbf{u}) = D_{ij}(\overline{\mathbf{u}}) + \widetilde{\tau_{ij}}(\mathbf{u})$ which, however, is inconvenient for modelling. Hence we use the approximation (exact for a plane water surface and bed geometry)

$$\begin{aligned}T_{ij}(\mathbf{u}) &= \widetilde{\overline{u_i u_j}} - \widetilde{\overline{u_i}}\,\widetilde{\overline{u_j}} \\ &\approx \widetilde{\widetilde{u_i}\widetilde{u_j}} - \widetilde{\overline{u_i}}\,\widetilde{\overline{u_j}} \\ &= \overline{D_{ij}(\mathbf{u})} + \tau_{ij}(\widetilde{\mathbf{u}})\end{aligned} \tag{9}$$

A model for the two-dimensional subgrid-scale stress $\tau_{ij}(\widetilde{\mathbf{u}})$ has to capture the inverse kinetic energy transfer typical for two-dimensional turbulence (Lesieur 1990). By splitting the instantaneous velocity into a mean-part and a fluctuating part $\mathbf{u} = \langle\mathbf{u}\rangle + \mathbf{u}'$, where $\langle\ldots\rangle$ is the time-average, we get a decomposition of $D_{ij}(\mathbf{u})$ (Hinterberger et al. 2002). The time-average is:

$$\langle D_{ij}(\mathbf{u})\rangle = D_{ij}(\langle\mathbf{u}\rangle) + \underbrace{\left\langle\widetilde{u_i' u_j'}\right\rangle - \left\langle\widetilde{u}_i'\widetilde{u}_j'\right\rangle}_{\langle D_{ij}(\mathbf{u}')\rangle} \tag{10}$$

The frist term, $D_{ij}(\langle\mathbf{u}\rangle)$ is caused by the mean velocity profile. The second term $\left\langle\widetilde{u_i' u_j'}\right\rangle$ represents the depth-averaged Reynolds stresses including all scales — the unresolved small-scale 3D fluctuations and the resolved 2D structures — while $\left\langle\widetilde{u}_i'\widetilde{u}_j'\right\rangle$ represents the Reynolds stresses caused by the 2D structures only. Therefore, the difference of both, $\langle D_{ij}(\mathbf{u}')\rangle$, can be interpreted as the Reynolds stresses of the 3D fluctuations. These observations motivate the model

$$\overline{D_{ij}(\mathbf{u})} \approx \overline{D_{ij}(\langle\mathbf{u}\rangle)} + \overline{D_{ij}(\mathbf{u}')} \tag{11}$$

In various computations with a cylinder in a shallow flow it turned out that the term $\overline{D_{ij}(\langle\mathbf{u}\rangle)}$ has only a small impact on the results (its derivative in space is small) so that it is neglected here. The dispersion term $\overline{D_{ij}(\mathbf{u}')}$ on one hand generates 2D fluctuations out of the 3D unresolved flow. These are essential for triggering fluid dynamical instabilities as illustrated below. On the other hand the unresolved 3D turbulence enhances momentum exchange which can be represented by an eddy viscosity model (EDV). The term $\tau_{ij}(\widetilde{\mathbf{u}})$ accounts for unresolved 2D structures. With the fine grid employed below it is of minor importance and mainly of dissipative character. For these two terms we introduce a combined model made up of an EVM and a stochastic back scatter model (BSM), the latter implemented through a random force F_i in the momentum equation:

$$\begin{aligned}\frac{\partial}{\partial x_j}T_{ij} &= \frac{\partial}{\partial x_j}\left(\overline{D_{ij}(\mathbf{u})} + \tau_{ij}(\widetilde{\mathbf{u}})\right) \\ &\approx \frac{\partial}{\partial x_j}\left(\overline{D_{ij}(\mathbf{u}')} + \tau_{ij}(\widetilde{\mathbf{u}})\right) \\ &\approx \frac{\partial}{\partial x_j}\left(-\nu_t 2\widetilde{\overline{S_{ij}}}\right) - F_i\end{aligned} \tag{12}$$

In the present simulations the water surface and the bottom wall are supposed to be flat (hence $h = const.$). This yields the model equations employed for the depth-averaged computations

$$\begin{aligned} \frac{\partial \widetilde{\overline{u_i}}}{\partial t} &+ \frac{\partial}{\partial x_j}\left(\widetilde{\overline{u_i}}\,\widetilde{\overline{u_j}}\right) = -\frac{\partial \Pi}{\partial x_i} \\ &+ \frac{\partial}{\partial x_j}\left((\nu+\nu_t)\,2\widetilde{\overline{S_{ij}}}\right) + F_i \\ &- \frac{c_f \widetilde{\overline{u}}_i \sqrt{\widetilde{\overline{u}}_k \widetilde{\overline{u}}_k}}{\rho h} \end{aligned} \tag{13}$$

where the pseudo pressure Π is determined to verify $\partial_{x_i}\widetilde{\overline{u_i}} = 0$. The generation of the force F_i for the BSM will be described in Section 3 below. For the eddy viscosity we use a model based on the local friction velocity and the water depth $\nu_t = c_h h u_\tau$.

2 3D-LES OF OPEN CHANNEL FLOW

A wide, straight open channel flow without horizontal shear can be regarded as a prototype situation for the study of the unresolved small scale turbulence which has to be modelled in a DA-LES. To obtain reference data we performed a highly resolved 3D-LES of an open channel flow with a Reynolds number based on the bulk velocity U and the water depth of $Re = Uh/\nu = 10935$ for which $Re_\tau = u_\tau h/\nu = 590$ based on the friction velocity, similar to the DNS of (Moser et al. 1999) for a closed channel flow. The size of the computational domain is $8\pi h$ in streamwise ($x-$axis) and $2\pi h$ in spanwise direction ($y-$axis), which allows to capture most of the larger 2D structures. Periodic boundary conditions are applied in spanwise and streamwise direction. The water surface is approximated by a rigid lid assumption, which is equivalent to a frictionless symmetry boundary. The numerical grid has 512 cells in streamwise, 256 in spanwise and 64 in vertical direction, yielding a resolution of $\Delta x^+ = 29$, $\Delta y^+ = 14.5$ in wall units. In the wall normal, vertical $z-$direction the grid has 3% stretching and a wall distance of about $\Delta z_P^+ = 1.5$ for the near-wall cell. At the wall, no-slip conditions are used.

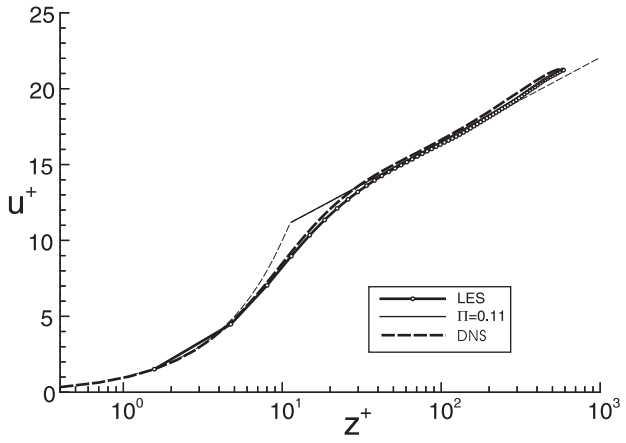

Figure 1: Nondimensional velocity in open channel flow $Re = 10935$ $(Re_\tau = 590)$; comparison of LES results with DNS of channel flow (Moser, Kim and Mansour 1999) and experimental relation $u^+ = 5.29 + 1/0.412 \ln(z^+)$ with Coles wake parameter $\Pi = 0.11$ (Nezu and Rodi 1986).

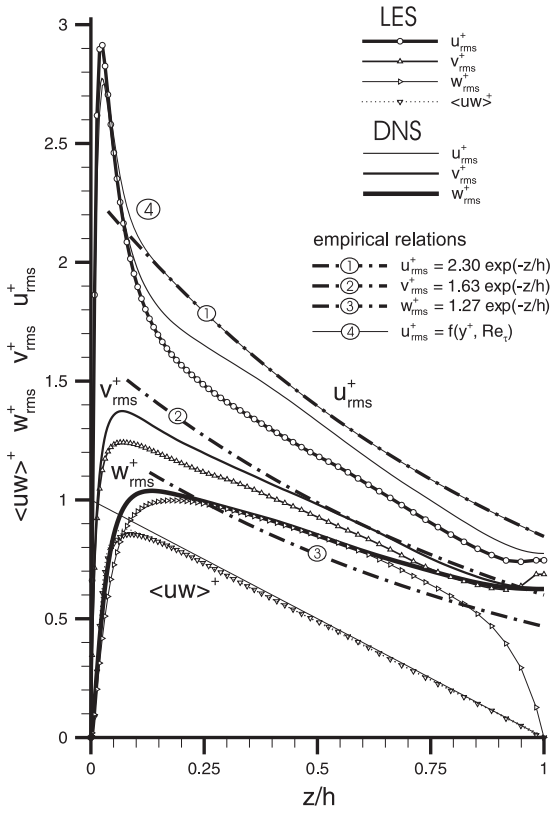

Figure 2: RMS-values of turbulent fluctuations and shear stress in open channel flow, $Re = 10\,935$; comparison of 3D-LES with empirical relations (Nezu and Nakagawa 1993) and DNS of channel flow (Moser, Kim and Mansour 1999).

Figure 1 shows the computed non-dimensional mean velocity profile and in Figure 2 the turbulent fluctuations are plotted. The velocity profile agrees very well with the measurements of (Nezu and Rodi 1986) and shows good agreement with the DNS results of (Moser et al. 1999) for one half of the closed channel. Open and half of closed channels can be compared as for physical reasons these are identical except near the free surface respectively the symmetry plane. At the free surface the fluctuations normal to the free surface (w'_{rms}) are damped and their energy is redistributed to the streamwise (u'_{rms}) and spanwise fluctuations (v'_{rms}). With this exception the velocity fluctuations of the LES agree well with the DNS data and experimental relations (Fig. 2).

The instantaneous streamwise velocity fluctuations u' at different depth levels are shown for one in-

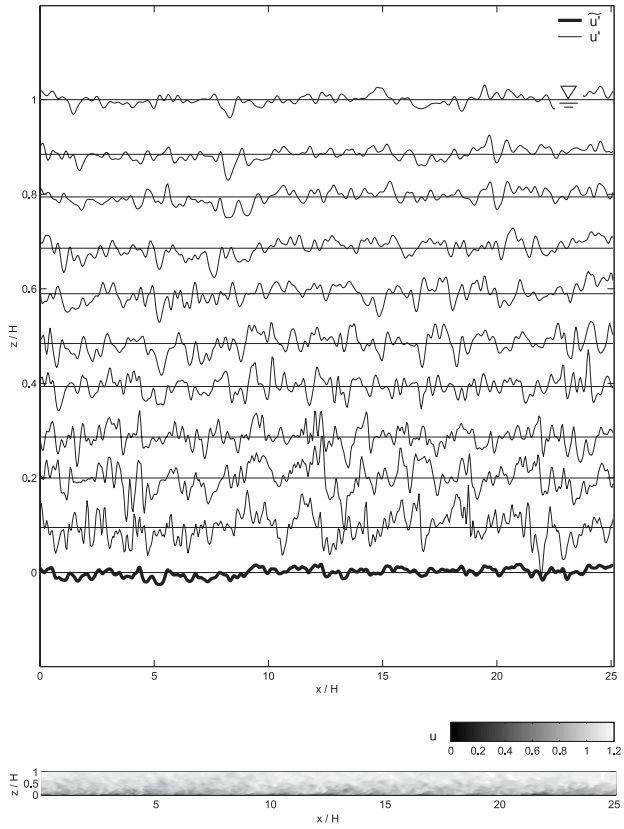

Figure 3: 3D-LES of open channel flow with $Re = 10935$ $(Re_\tau = 590)$; top: — streamwise velocity fluctuations $u'(x, y, z)$ (with $y = const.$, $z/h = const.$) in different water depth levels and resulting fluctuations of depth averaged velocity $\widetilde{u}'(x)$ (thick line plotted at the bed $z/h = 0$), bottom: contour plot of the related streamwise velocity field in x-z-plane.

stant in Figure 3 along lines in $x-$direction, all at the same spanwise position. When this three-dimensional motion is depth-averaged, there still remain two-dimensional fluctuations. These are illustrated by the lowest signal in Figure 3 representing $\widetilde{u}'$, i.e. the depth-average of the signals shown above. The fluctuations of the other depth-averaged velocity components $\widetilde{v}'$ and $\widetilde{w}'$ (not shown here) look similar. From such 3D simulations we have deduced

$$\widetilde{k} = \frac{1}{h}\int_h \frac{1}{2}\left(\langle uu\rangle + \langle vv\rangle + \langle ww\rangle\right) dz \approx 1.8 \cdot u_\tau^2 \quad (14)$$

as an approximation of the depth-averaged kinetic energy. For the kinetic energy of the depth-averaged motion we find

$$k_{2d} = \frac{1}{2}\left(\langle \widetilde{u}'\widetilde{u}'\rangle + \langle \widetilde{v}'\widetilde{v}'\rangle\right) \approx 0.25 \cdot u_\tau^2 \qquad (15)$$

Hence, in a turbulent open channel flow without horizontal shear the depth-averaged 2D motion caused by small scale turbulence contains approximately 15% of the depth-averaged kinetic energy. Furthermore,

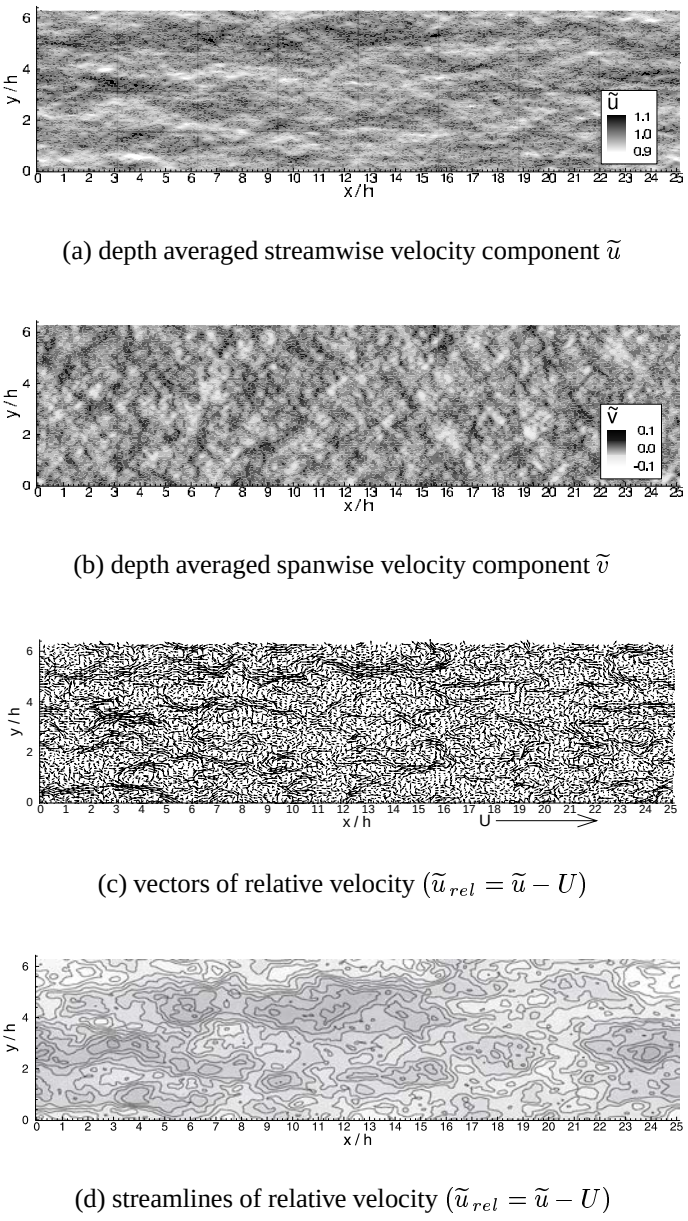

(a) depth averaged streamwise velocity component $\widetilde{u}$

(b) depth averaged spanwise velocity component $\widetilde{v}$

(c) vectors of relative velocity $(\widetilde{u}_{rel} = \widetilde{u} - U)$

(d) streamlines of relative velocity $(\widetilde{u}_{rel} = \widetilde{u} - U)$

Figure 4: Depth averaged velocities in open channel flow; 3D-LES $Re = 10935$ $(Re_\tau = 590)$.

large-scale structures are present as illustrated in Figure 4. It shows the depth-averaged velocity components and the relative velocities, observed when moving with the bulk velocity U. The structures typically have a streamwise extent of more than 10 water-depths, but their size is limited by the size of the computational domain as revealed by the computed spatial correlations.

3 BACK SCATTER MODEL

In a developed open channel flow with no horizontal shear of the mean flow all 2D turbulent motion is caused by the bottom-generated turbulence as discussed in the previous section. Also in more general flows this contribution can be important as illustrated by the computations below. For this reason the energy

transfer from the unresolved 3D turbulence to the resolved 2D turbulence needs to be modelled. For the production rate P_{2d} of 2D turbulent kinetic energy we assume

$$P_{2d} \sim \frac{P_{3d}}{Re_\tau} = \frac{|\widetilde{\mathbf{u}}| \cdot u_\tau^2}{h \cdot Re_\tau} = \frac{|\widetilde{\mathbf{u}}|^2 \nu \sqrt{c_f}}{h^2} \qquad (16)$$

This production rate is represented by the BSM implemented through the 2D force

$$\mathbf{F} = F_{rms} \cdot \mathbf{Z}/Z_{rms} \qquad (17)$$

Here, $\mathbf{Z}$ is a random vector field with zero mean and F_{rms} a scaling factor adjusting the root mean square ($F_{rms} = \sqrt{F_{1rms}'^2 + F_{2rms}'^2}$) to the desired value. The production of 2D kinetic energy by this force, updated each time step, is

$$P_{2d} \sim F_{rms}^2 \cdot \Delta t \qquad (18)$$

where Δt is the size of the time step (Alvelius 1999). Combining Equation 16 and 18 yields

$$F_{rms} = c_B \cdot \sqrt{\frac{P_{2d}}{\Delta t}} = c_B \cdot \frac{|\widetilde{\mathbf{u}}|}{h} \sqrt{\frac{\nu\sqrt{c_f}}{\Delta t}} \qquad (19)$$

The model constant c_B is adjusted to obtain the level of 2D kinetic energy given by Equation 15.

Apart from the scaling factor, the random field $\mathbf{Z}$ needs to be determined. The spectral properties of this field are essential for the performance of the BSM. For numerical and physical reasons, it is preferable to apply a force field which is divergence free. With a free surface e.g. a divergence in this field could cause unphysical oscillations of the water level. One method to compute a solenoidal random vector field $\mathbf{Z}$ is to perform a projection step according to $\mathbf{Z} = \mathbf{Z}^{div} - \nabla\varphi$, where $\mathbf{Z}^{div}$ is an arbitrary random vector field and φ the solution of $\nabla^2\varphi = \nabla \cdot \mathbf{Z}^{div}$ (Schumann 1995). Solving an additional Poisson equation, however, is numerically expensive. A cheaper approach is to use the rotation of a random vector potential $\mathbf{\Phi}$ to derive a solenoidal field $\mathbf{Z} = \nabla \times \mathbf{\Phi}$ (Leith 1990; Mason and J.Thomson 1992). In the 2D case this is equivalent to the use of a random stream function Ψ such that $Z_1 = \partial_y \Psi$ and $Z_2 = -\partial_x \Psi$. We implemented and tested this approach, but found unsatisfactory results. The reason is that the spatial derivatives of the stream function amplify the fine-scale components of Ψ, and moreover do so in an anisotropic way.

In the LES simulations according to Equation 13 a divergence of $\mathbf{F}$ has no influence on the velocity field and is compensated by a modified pressure field $P = p + p^*$ (with $\nabla^2 p^*/\rho = \nabla \cdot \mathbf{F}$). In fact the projection step to render the force field divergence free is then done by the pressure solver. This causes some extra cost in an iterative pressure correction step but allows to use a non-solenoidal force. We found that removing the very high and the low temporal and spatial frequencies of $\mathbf{F}$, as detailed below, is much more important for numerical stability and for the quality of the results than using a divergence-free field.

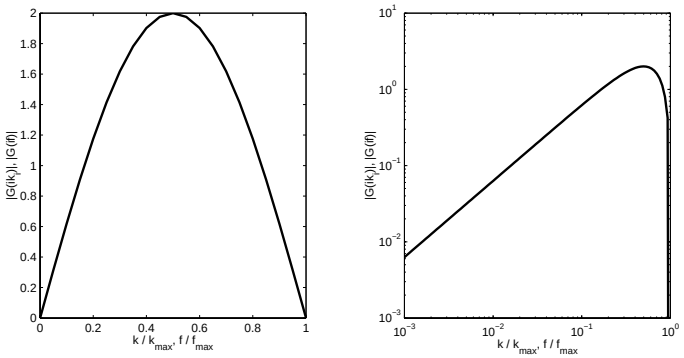

Figure 5: Transfer function of bandpass filter in linear and double-logarithmic scaling.

The spectral properties of $\mathbf{F}$ are adjusted by computing

$$\mathbf{Z}(\mathbf{x}, t) = \overline{\mathbf{r}(\mathbf{x}, t)}^{BSM} \qquad (20)$$

based on a random white noise vector field $\mathbf{r}(\mathbf{x}, t)$ with a standard normal distribution. The filter operator $\overline{}^{BSM}$ is different from the LES filter. For a structured cartesian grid, with spatial indices I,J and temporal index N, this filter in space and time is implemented as

$$(Z_i)_{I,J}^N = \sum_{q=-n}^{n} \sum_{r=-n}^{n} \sum_{s=-n}^{n} a_q\, b_r\, c_s \cdot (r_i)_{I-r,J-s}^{N-q} \qquad (21)$$

where the coefficients a_q, b_r, c_s introduce filtering of order up to $2n$. When r_i is white noise the spectrum of the forces $\hat{\mathbf{F}}(\mathbf{k}, f)$ is proportional to the transfer function of the filter

$$\begin{aligned} \hat{G}(\mathbf{k}, f) \;=\; & \sum_{q=-n}^{n} \sum_{r=-n}^{n} \sum_{s=-n}^{n} (a_q b_r c_s \cdot \\ & \cdot \quad e^{-\imath(q\, 2\pi f \Delta t + r\, k_1 \Delta x + s\, k_2 \Delta y)}) \end{aligned} \qquad (22)$$

The norm of the filter determines the scaling coefficient

$$(Z_i)_{rms} = \sqrt{\sum_{q=-n}^{n} a_q^2 \cdot \sum_{r=-n}^{n} b_r^2 \cdot \sum_{s=-n}^{n} c_s^2} \qquad (23)$$

We obtained a reasonable model with a simple temporal and spatial bandpass filter of second order, which is obtained with $n = 1$, $a_1 = -1$, $a_0 = 0$, $a_1 = 1$, and $\mathbf{a} = \mathbf{b} = \mathbf{c}$. This grid-based filter depends on the time step and the grid resolution. It has a temporal cutoff frequency of $f_{max} = 1/(2\Delta t)$ and the cutoff

wave numbers $k_{1\,max} = \pi/\Delta x$ and $k_{2\,max} = \pi/\Delta y$ in space. The transfer function of this filter and hence the spectrum $\hat{\mathbf{F}}(\mathbf{k}, f)$ is shown in Figure 5. Low and high frequencies are damped as desired. The logarithmic plot shows, that the forcing occurs mainly at the higher resolved frequencies and wave numbers. It is proportional to $\mathbf{k}$ at lower spatial wave numbers and proportional to f at the lower temporal frequencies.

4 SHALLOW MIXING LAYER

In this section we consider a shallow mixing layer as studied by Chu and Babarutsi (Chu and Babarutsi 1988), experiment No. 4. The flume has a width of $61\,cm$, the water depth is $2.96\,cm$, the inflow velocities are $U_1 = 26.4\,cm/s$ and $U_2 = 11.1\,cm/s$. The Reynolds number based on the bulk velocity $U = (U_1 + U_2)/2 = 18.75\,cm/s$ and the water depth is $Re = 5\,550$. Figure 6 shows the computational domain and the boundary conditions. The simulations are performed in nondimensional form: the lengths are normalized by the water depth and the velocities by the bulk velocity. In two periodic regions (P1 and P2) a fully developed turbulent open channel flow with side walls is computed. These periodic regions act as turbulent inflow generators providing data for the inflow boundaries located 10 water depths upstream of the end of the splitter plate. A convective outflow boundary is located at $x \approx 155h$. To improve numerical stability and the convergence rate of the pressure solver a damping region is placed in front of the outflow boundary where the viscosity is increased by a factor of 10. The computational grid consists of 16 blocks, which can be distributed to 16 processors. Due to limited computing resources and the large horizontal extent the grid resolution possible for a 3D-LES does not allow to resolve the viscous sublayers near the walls. In contrast to the simulation of the open cannel flow described before, wall functions have to be used here. The wall function applied is similar to the Werner-Wengle approach (Werner 1991), but assumes an instantaneous logarithmic profile instead of a power law profile. To limit the computational expense $\Delta x = \Delta y = \Delta z = 0.1h$ was selected. The center of the wall adjacent cell is at $\Delta z_P^+ \approx 15$. The resulting computational grid used for the 3D-LES has $2.6 \cdot 10^6$ interior grid cells. For the DA-LES a

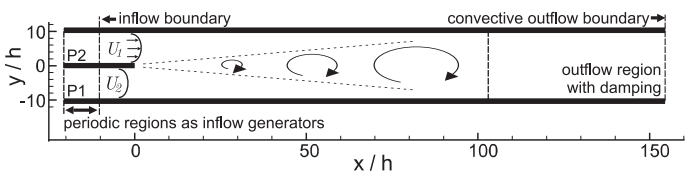

Figure 6: Shallow mixing layer; computational domain and boundary conditions for 3D-LES and DA-LES.

coarser horizontal resolution with $\Delta x = \Delta y = 0.2h$ was chosen, resulting in $66\,000$ interior cells.

In Figure 7 the mean streamwise velocity at half the water depth and the fluctuations of the streamwise velocity computed with the 3D-LES are compared with the experimental data of Chu and Babarutsi (Chu and Babarutsi 1988). The spreading rate in the experiment is much larger than computed by the LES. This is a consequence of differences in the inflow conditions: In the LES the inflow is fully developed while in the experiment the inflow region is rather short and the flow presumably not fully developed. This is backed by the u'_{rms} fluctuations at $x = 0.3h$. Here, the LES shows fluctuations which are typical for a fully developed open channel flow but the experiment shows lower levels. Uijttewaal and Booij (Uijttewaal and Booij. 2000) also found a much smaller spreading rate in similar experiments as Chu and Babarutsi and pointed out that different conditions at the end of the splitter plate can have a dominant effect on the further development of the mixing layer (Bell and Mehta 1990).

For the visualisation of vortex structures in the computation the low-velocity stream of the mixing layer was coloured by a passive tracer. Therefore an additional scalar transport equation was solved, using the HLPA convection scheme (Zhu 1991). The mixing of this tracer is shown in Figure 8 for different cases. The large-scale structures which dominate the horizontal mixing can be seen clearly. For the three-dimensional LES the tracer concentration is shown at three different depths $z/h = 0.05$, 0.55 and

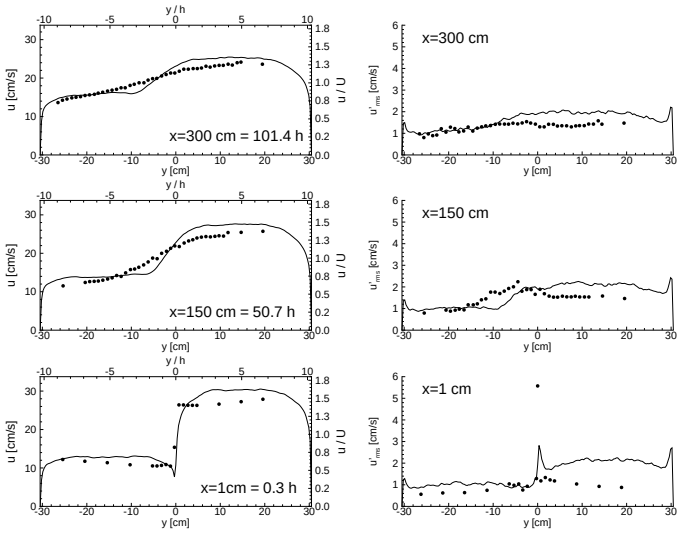

Figure 7: Mean streamwise velocity $\langle u \rangle$ (left) and RMS values of streamwise velocity fluctuations u'_{rms} (right) at different downstream locations of the mixing layer in half of the water depth; comparison of 3D-LES results with experimental data (scanned from Babarutsi and Chu and Babarutsi 1998)

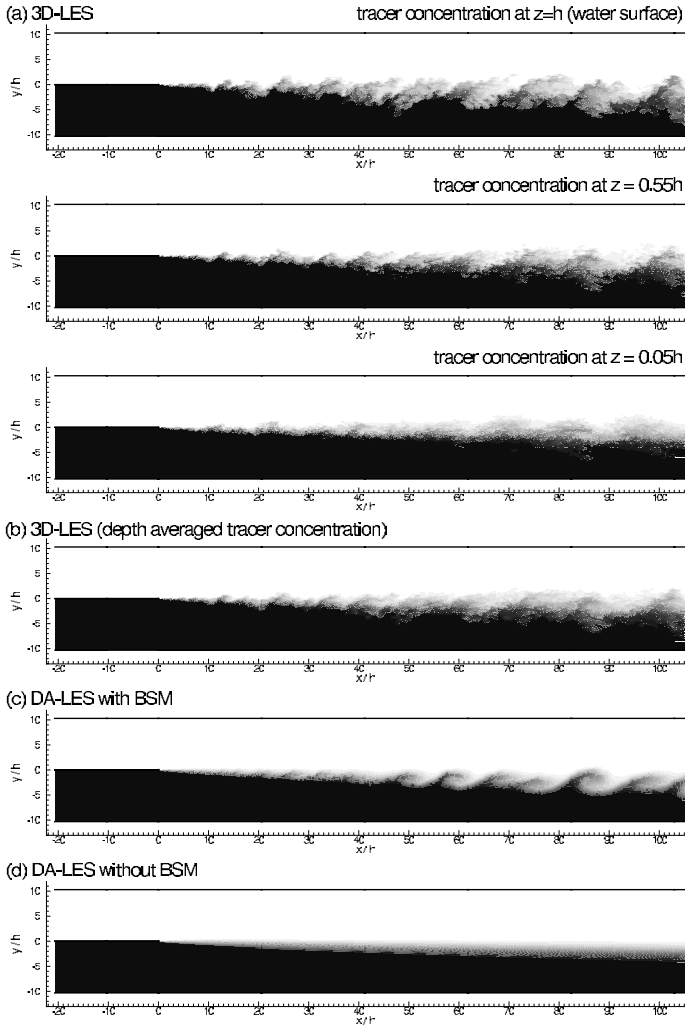

Figure 8: Mixing layer computed with 3D-LES and DA-LES. A passive tracer is introduced in the low-velocity stream; a: 3D-LES tracer concentration at the water surface; b: 3D-LES depth averaged tracer concentration; c: DA-LES with backscatter model ($c_h = 0.08$, $c_B = 55$); d: DA-LES without backscatter model ($c_h = 0.08$, $c_B = 0$).

1.0 (Fig. 8 a). While the two-dimensional structures are large close to the water surface these are rather weak and small near the bed. The structures show a shift over the different water levels due to the different mean velocity at different levels. This shift and the smaller structures close to the channel bed result in a blurred picture when looking at the depth-averaged tracer concentration (Fig. 8 b). The latter is the target for the DA-LES. Similar 2D structures can be observed in the results of the DA-LES with back scatter model (Fig. 8 c). The model constants, $c_h = 0.08$ and $c_B = 55$, were adjusted to yield an adequate representation of the large-scale dynamics and that k_{2d} in the inflow plane matches the 3D results (Fig. 9 bottom). Without the back scatter model the DA-LES fails to predict a turbulent 2D motion and the flow is steady. The horizontal shear is too weak to develop

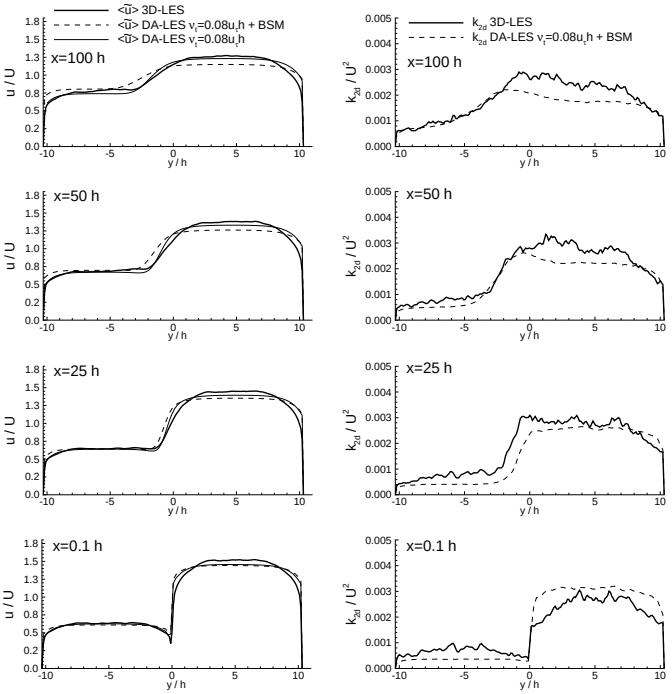

Figure 9: Results of 3D-LES (thick line) compared with DA-LES with back scatter model (dashed line) and DA-LES without BSM (thin line) at different downstream locations of the mixing layer; left: depth averaged streamwise mean velocity $\langle\tilde{u}\rangle$; right: kinetic energy of 2D turbulence $k_{2d} = \frac{1}{2}\left(\langle\tilde{u}'\tilde{u}'\rangle + \langle\tilde{v}'\tilde{v}'\rangle\right)$ (k_{2d} of DA-LES without BSM is zero).

any 2D fluctuations and no coherent structures are present (Fig. 8 d). As a consequence the spreading rate is substantially underpredicted. This can be seen in the computed depth-averaged streamwise mean velocity profiles, which are shown together with the 2D kinetic energy in Figure 9 at different downstream locations. There are no depth-averaged data available from the experiments, but the related depth-averaged 3D-LES data is plotted for comparison. While the DA-LES without BSM yields no 2D kinetic energy at all, the DA-LES with BSM shows a very good agreement with the 3D-LES data over the whole flow field, but there are noticeable discrepancies in the mean velocity profiles and in the spreading rate. Close to the end of the splitter plate there is only a very small difference in the velocity profiles between the DA-LES with and without BSM, but a noticeable difference to the depth-averaged 3D-LES data. This shows that the fluctuations generated by the BSM have a minor effect on the computed mean flow field in the upstream region, and that here the EVM is responsible for the observed velocity profiles.

5 CONCLUSIONS

The presented 3D-LES of a wide, straight open channel flow shows large streamwise coherent structures which result from the small-scale turbulence generated at the bottom. The energy of the 2D fluctuations

which are present in developed turbulent open channel flow even in the absence of horizontal shear of the mean flow plays an important role in the development of mixing layers and has to be modelled when performing depth-averaged LES simulations. We introduced a simple back scatter model which generates an appropriate random forcing term. This model is able to generate 2D kinetic energy in good agreement with a corresponding 3D-LES. The coherent structures predicted in a DA-LES with BSM agree quite well with the 3D-LES results, while a DA-LES without the BSM showed no 2D turbulent motion at all. The current results are promising and the model will be applied to other configurations in further studies.

6 ACKNOWLEDGEMENT

This research has been supported by the DFG (Ro558/18 and Ro558/16). The authors thank B. van Prooijen for interesting discussions on the subject of this paper.

REFERENCES

Alvelius, K. (1999). Random forcing of three-dimensional homogeneous turbulence. *Physics of Fluids 11*(7), 1880–1889.

Babarutsi, S. and V. H. Chu (1998). Modelling transverse mixing layer in shallow open–channel flows. *J. Hydr. Engrg. 124 (7)*, 718–726.

Bell, J. H. and R. D. Mehta (1990). Developement of a two-stream mixing layer from tripped and untripped boundary layers. *AIAA J.* (2034).

Chu, V. H. and S. Babarutsi (1988). Confinement and bed–friction effects in shallow turbulent mixing layers. *J. Hydr. Engrg. 114 (10)*, 1257–1274.

Ferziger, J., J. Koseff, and S. Monismith (2002). Numerical simulation of geophysical turbulence. *Computers & Fluids 31*, 557–568.

Guirk, J. M. and W. Rodi (1978). A depth-averaged mathematical model for the near field of side discharges into open channel flows. *J. Fluid Mech. 86*(part 4), 762–781.

Hinterberger, C., J. Fröhlich, and W. Rodi (2002). Depth-averaged large eddy simulation of shallow water flows - modelling aspects. In I. Castro, P. Hancock, and T. Thomas (Eds.), *Advances of Turbulence IX, Proceedings of 9th European Turbulence Conference*, Barcelona, pp. 211–214. CIMNE.

Leith, C. E. (1990, 3). Stochastic backscatter in a subgrid-scale model: Plane shear mixing layer. *Phys. Fluids A 2*, 297–299.

Lesieur, M. (1990). *Turbulence in Fluids, Stochastic and Numerical Modelling*. Kluwer Academic Publishers.

Madsen, P., M. Rugbjerg, and I. Warren (1988). Shallow-water turbulence modelling and horizontal large-eddy computation of river flow. *J. Hydraulic Eng. 124*, 493–500.

Mason, P. J. and D. J.Thomson (1992). Stochastic backscatter in large-eddy simulations of boundary layers. *J. Fluid. Mech. vol. 242*, 51–78.

Moser, R. D., J. Kim, and N. N. Mansour (1999). Direct numerical simulation of turbulent channel flow up to $Re_\tau = 590$. *Physic of Fluids 11 (4)*, 943–945.

Nadaoka, K. and H. Yagi (1998). Shallow-water turbulence modelling and horizontal large-eddy computation of river flow. *J. Hydr. Engr.*, 493–500.

Nezu, I. and H. Nakagawa (1993). *Turbulence in Open–Channel Flows*. A.A. Balkema.

Nezu, I. and W. Rodi (1986). Open-channel flow messurements with a laser Doppler anemometer. *J. Hydraulic Eng., ASCE 112*, 335–355.

Schumann, U. (1995). Stochastic backscatter of turbulence energy and scalar variance by random subgrid-scale fluxes. *Proc. R. Soc. Lond. A* (451), 293–318.

Uijttewaal, W. S. J. and R. Booij. (2000, February). Effects of shallowness on the development of free-surface mixing layers. *Physics of Fluids 12*(2), 392–402.

van Prooijen, B. C. and W. S. J. Uijttewaal (2002). On the initiation of large scale turbulence structures in the numerical simulation of shallow mixing layers. In D. Bousmar and Y. Zech (Eds.), *River Flow 2002 - Proceedings of the International Conference on Fluvial Hydraulics*, Number ISBN 90 5809 509 6. Swets & Zeitlinger, Lisse, The Netherlands.

van Vossen, B. (2000, Aug.). *Horizontal Large Eddy Simulations; evaluation of flow computations with Delft3D-Flow*. Ph. D. thesis, Delft University of Technology.

Werner, H. (1991). *Grobstruktursimulation der turbulenten Strömung über eine querliegende Rippe in einem Plattenkanal bei hoher Reynoldszahl*. Ph. D. thesis, Universität München.

Zhu, J. (1991). A low diffusive and oscillation-free convection scheme. *Commun. Appl. Num. Meths 7*, 225–232.